

Cantilever Snap-Fit Performance Analysis for Haptic Evaluation

Jingjing Ji

Department of Mechanical Engineering,
Zhejiang University,
Hangzhou 310027, China

Kok-Meng Lee

Woodruff School of Mechanical Engineering,
Georgia Institute of Technology,
Atlanta, GA 30332-0405
e-mail: kokmeng.lee@me.gatech.edu

Shuyou Zhang¹

Department of Mechanical Engineering,
Zhejiang University,
Hangzhou 310027, China
e-mail: zsy@zju.edu.cn

This paper investigates the parametric effects, which include material properties, hook shape, and shear deformation, on the force/deflection relationship governing the assembly/disassembly processes of a snap-fit for developing embedded algebraic solutions to achieve realistic force feedback through a haptic device. For this purpose, an algebraic model, which isolates individual parametric factors that contribute to the cantilever hook deflection, has been derived for examining assumptions commonly made to simplify models for design optimization and real-time control. The algebraic model has been verified by comparing computed results against those simulated using ANSYS FEA workbench and published approximate solutions. Additionally, the model has been validated by comparing the friction coefficients of three different snap-fit designs (with same materials), which closely agree within 5% of their root-mean-square value. Implemented on a commercial PHANTOM haptic device, we demonstrate the effectiveness of the model as embedded algebraic solutions for haptic rendering in design. Nine individuals participated in evaluating a set of design options with different parameter settings; 78% of whom chose the optimal theoretical solution by feeling the feedback force. These findings demonstrate that the design confidence of assembly robustness can be enhanced through a relatively accurate virtual force feedback. [DOI: 10.1115/1.4005085]

Keywords: snap-fit, cantilever hook, assembly, disassembly, virtual force feedback, haptics, psychophysics

1 Introduction

Snap-fits are widely used in various types of products, equipments, and power systems to provide attachment functionality in assemblies as they can be incorporated as feature molded in parts thus reducing part count; and their ease of assembly and disassembly lowers manufacturing cost and time. Snap-fits performance analysis requires not only the virtual simulation results but also a good understanding of the inherent motion/force transmission through deformation encountered during assembly, in which a sense of human touch to feel the level of contact force is needed. Motivated by the emerging haptic technology that helps humans feel the sense of touch, this paper develops an analytical model for enhancing performance analysis in virtual manufacturing.

Traditionally, snap-fits were designed based on classical mechanical knowledge; for example, Bonenberger [1] offered a comprehensive description for analyzing snap-fits assembly and disassembly, in Refs. [2–4] linear beam theory was introduced, and in Ref. [5] a method for attachment design concept in integral snap-fit assembly was proposed. Recently, finite element methods (FEMs) have been widely used to obtain accurate numerical solutions [6–9]. In general, FEMs are computationally time demanding, which motivate engineers to concentrate on model optimization and dimension reduction to overcome the high computational expense. In Ref. [8], a computational model using nonlinear constrained minimization was presented to efficiently design flexible fingers subjected to large deflection without loss of accuracy, where the theoretical accuracy was verified by comparing to simulated results against FEM. A nonlinear algebraic reduction method was proposed in Ref. [9] to offer the generality of 3D simulation and the computational efficiency of 1D simulation.

Snap-fits offer resistance to engagement during the assembly and disassembly processes. Experiment fixtures were used in Ref. [10] to provide the force and tactile feedback in preloaded cantile-

ver snap-fits under manual assembly for applications in the automotive industry, where force/tactile feedback is essential for sensing the full engagement of snap-fit parts during the assembly of critical components (such as electrical and fuel system interconnects). The findings in Ref. [10] have motivated us to explore extending the method by incorporating haptic rendering, which offers designers useful feedback force as they assemble snap-fits, to enhance product design involving snap-fits in virtual environment. Haptic technology, which has been widely introduced to machine, robot automation, biotechnology, and medical product design assessment [11–15], could provide feedback force to enable designers to experience the deformation in virtual environment, thereby allowing them to make objective evaluation of product performance. However, accurate solutions that can be embedded in haptic technology to provide real-time force/displacement feedback in virtual design environment are required to provide confidence of assembly robustness that can be enhanced in industrial settings.

For the above reasons, this paper examines the parametric effects (which include material properties, hook shape, and shear deformation) on the force/deflection relationship governing the design of a snap-fit. Along with a relatively complete model (CM), this investigation provides a basis for developing embedded algebraic solutions that can be efficiently implemented to achieve realistic force feedback through a haptic device when optimizing design geometry of snap-fits in real time. The remainder of this paper offers the following:

- (1) In the context of snap-fits, a relatively complete algebraic model for analyzing both assembly and disassembly of a snap-fit is presented. With real-time haptic evaluation of designs in mind, this model isolates individual parametric factors that contribute to the cantilever hook deflection. Thus, the algebraic model provides an effective means to examine assumptions often made to reduce models to tractable form for design optimization and real-time control. The relation between feedback force and deflection has been deduced to illustrate both assembly and disassembly of a snap-fit; several commonly used simplified models are compared.

¹Corresponding author.

Contributed by the Design Theory and Methodology Committee of ASME for publication in the JOURNAL OF MECHANICAL DESIGN. Manuscript received February 13, 2011; final manuscript received August 28, 2011; published online December 9, 2011. Assoc. Editor: John K. Gershenson.

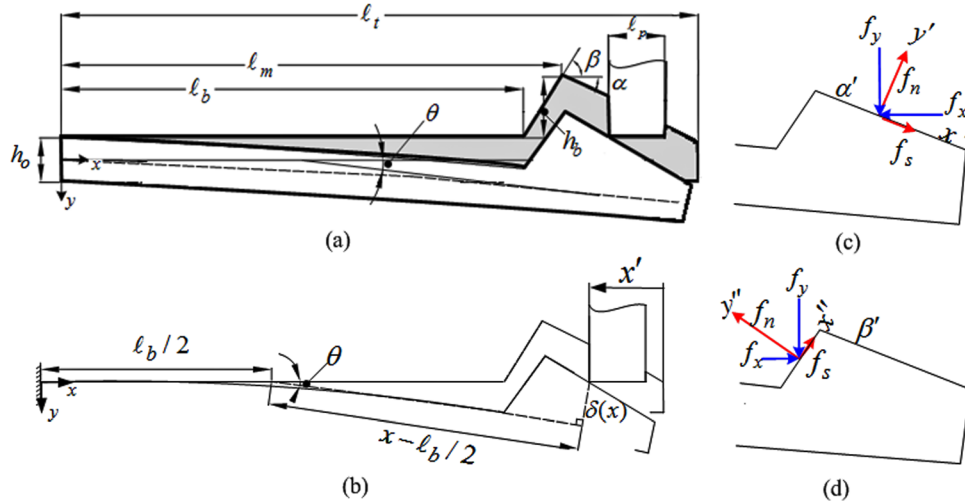


Fig. 1 Cantilever hook and matching part; (a) coordinate systems and characteristic dimensions, (b) sketch illustrating deflection, (c) forces components in insertion, and (d) forces components in retention

- (2) The proposed model has been verified with two methods. This first method compares computed results against those simulated using ANSYS FEA workbench and published approximate solutions. The second method uses a coupled calculation/measurement approach to determine and compare the friction coefficients of three different snap-fit designs (with same materials), which closely agree within 5% of their root-mean-square value.
- (3) Implemented through a commercial PHANTOM haptic device [16], we demonstrate the effectiveness of the inverse model (as embedded algebraic solutions) for use in haptic rendering in design processes, where real-time virtual force feedback is essential.

2 Analytical Model

Figure 1 illustrates the snap-fit assembly of a typical cantilever hook (base thickness h_o , width w , and length l_t) with a wedge-shaped end characterized by the height h_b and angles (α, β) , where the shaded cantilever indicates its initial state, and δ is the beam deflection as the matching part contacts the wedge at x . As the matching part advances (or retracts) for assembly (or disassembly), the contact point slides along the front (or rear) surface of the wedge as well as deflects the beam.

Without loss of generality, the following geometries are considered: $x = [0, l_t]$, $\alpha, \beta = [0, \pi/2]$, and

$$h(x) = \begin{cases} h_o, & \text{for } x = [0, \ell_b] \\ h_o + (x - \ell_b) \tan \beta, & \text{for } x = [\ell_b, \ell_m]; \beta = [0, \pi/2] \\ h_o + (\ell_t - x) \tan \alpha, & \text{for } x = [\ell_m, \ell_t]; \alpha = [0, \pi/2] \end{cases} \quad (1)$$

In Eq. (1), $h(x) = h_o + h_b$ when $\alpha = \pi/2$ ($\ell_m = \ell_t$) or $\beta = \pi/2$ ($\ell_b = \ell_m$). The following derivation focuses on assembly; the process starts from $(x, y) = (\ell_t, -h_o/2)$. To offer intuitive insights to facilitate design, we normalize the forces to (Ewh_o) and geometrical dimensions to h_o as follows:

$$\begin{bmatrix} F_x \\ F_y \end{bmatrix} = \frac{1}{Ewh_o} \begin{bmatrix} f_x \\ f_y \end{bmatrix}; \quad X = \frac{x}{h_o}; \quad L_b = \frac{\ell_b}{h_o}; \quad H_b = \frac{h_b}{h_o}; \quad L_t = \frac{\ell_t}{h_o}$$

The snap-fit assembly (moving from $x = \ell_t$ in the $-x$ direction) consists of three processes: insertion, dwelling, and retention.

- During insertion (Fig. 1(c)), the matching part moves up along the inclined surface of the wedge (against a downward

friction) as the cantilever deflects and reaches its maximum deflection at $x = \ell_m$.

- The matching part slides on the tip while maintaining its maximum deflection during dwelling.
- The elastic deformation gradually returns to zero as the matching part moves down the inclined surface completing the retention process (Fig. 1(d)). Unlike insertion, the frictional force is upward during retention.

The contact force $(f_n, f_s = \mu f_n)$ is resolved into x and y components so that solutions presented here can be compared against those commonly used in snap-fit design for product assembly. From the equilibrium of forces in the x and y directions as illustrated in Figs. 1(c) and 1(d)

$$\begin{bmatrix} \pm f_s \\ f_n \end{bmatrix} = \begin{bmatrix} \cos \gamma' & -\sin \gamma' \\ \sin \gamma' & \cos \gamma' \end{bmatrix} \begin{bmatrix} f_x \\ f_y \end{bmatrix} \quad (2a)$$

$$\text{where } \gamma' = \begin{cases} \alpha' = \alpha + \tan^{-1}(\delta/x), & \text{for } x = [\ell_m, \ell_t] \\ \beta' = \beta - \tan^{-1}(\delta/x), & \text{for } x = [\ell_b, \ell_m] \end{cases}$$

In Eq. (2a), $+f_s$ and $-f_s$ refer to insertion and retention, respectively. Solving Eq. (2a), the assembly force f_x and deflecting force

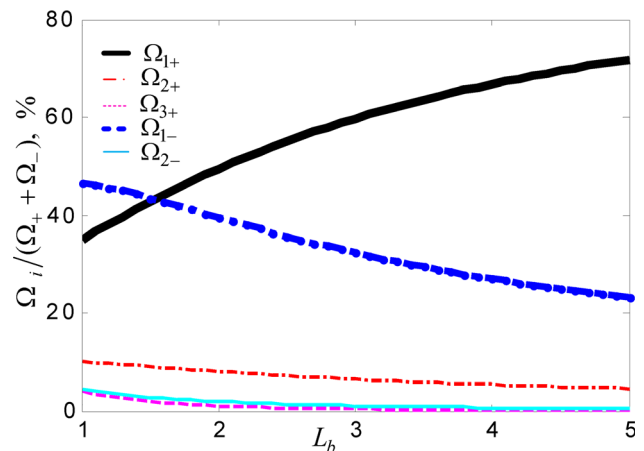


Fig. 2 Ω_i as a percentage of $(\Omega_+ + \Omega_-)$

f_y are related by Eq. (2b), where μ is the friction coefficient between the two sliding surfaces

$$\frac{f_x}{f_y} = \begin{cases} \tan(\gamma' + \tan^{-1} \mu) & \text{Insertion} \\ \mu & \text{Dwelling} \\ \tan(\gamma' - \tan^{-1} \mu) & \text{Retention} \end{cases} \quad (2b)$$

2.1 Deflection Formulation. The assembly of a snap-fit can be considered as a nonlinear beam deflection problem with the movement of the matching part as an input (that leads to the changing contact position on the inclined surfaces of the cantilever hook). The beam deflection δ can be expressed as

$$\delta = \delta_+ + \delta_- \quad (3)$$

where δ_+ and δ_- are due to f_y and f_x , respectively, and the subscripts “+” and “-” indicate the deflections are in the +y and -y directions, respectively. Derived using Timoshenko beam theory (that takes into account shear deformation) with Castigliano’s method, δ_+ and δ_- are given by Eqs. (3a) and (3b)

$$\delta_+ = \frac{\partial V_\varepsilon}{\partial f_y} \quad (3a)$$

$$\delta_- \approx \frac{1}{2}x\theta = \frac{1}{2}x \frac{\partial(\Delta V_\varepsilon)}{\partial M} \quad (3b)$$

2.1.1 Deflection Due to Vertical Force Component. The strain energy due to f_y is given by Eq. (4)

$$V_\varepsilon = \int_0^x \frac{(f_y x)^2}{2EI} dx + \int_0^x \frac{k f_y^2}{2GA} dx \quad (4)$$

where E and G are the Young’s modulus and shear modulus of the beam material; A and I are the cross-sectional area and its moment of the beam; and k is a dimensionless coefficient related with the section shape ($k=6/5$ for rectangular cross-section). The normalized deflection ($\Delta_+ = \delta_+/h_o$) is a function of F_y and can be expressed in the form of mechanical impedance

$$\Omega_+ = \frac{\Delta_+}{F_y} = \sum_{i=1}^3 \Omega_{i+} \quad (5)$$

$$\text{where } \Omega_{1+} = 4KL_b^3 \quad (5a)$$

$$\Omega_{2+} = \int_{\ell_b}^x \frac{12x^2 dx}{h^3(x)} \quad (5b)$$

$$\Omega_{3+} = \frac{kE}{G} \int_{\ell_b}^x \frac{dx}{h(x)} \quad (5c)$$

$$K = 1 + \frac{0.3}{L_b^2} \left(\frac{E}{G} \right) \quad (5d)$$

During dwelling, the matching part simply slides along the tip.

2.1.2 Deflection Due to the Moment Induced by the Horizontal Force. The strain energy induced by the component force f_x which results in a bending moment M in the beam is given by Eq. (6)

$$\Delta V_\varepsilon = \frac{1}{2E} \int_0^x \frac{M^2}{I(x)} dx \quad (6)$$

where

$$M = f_x \left(\frac{h_o}{2} + h_x \right) \text{ and } h_x = \begin{cases} (\ell_t - x) \tan \alpha, & \text{for } x = [\ell_m, \ell_t] \\ (x - \ell_b) \tan \beta, & \text{for } x = [\ell_b, \ell_m] \end{cases}$$

Substituting Eq. (6) into Eq. (3b) leads to Eq. (7), the normalized deflection ($\Delta_- = \delta_-/h_o$) in Eq. (3b) becomes

$$\Omega_- = \frac{\Delta_-}{sF_x} = \Omega_{1-} + \Omega_{2-} \quad (7)$$

$$\Omega_{1-} = 6X \left(H_x + \frac{1}{2} \right) L_b \quad (7a)$$

$$\Omega_{2-} = 6X \left(H_x + \frac{1}{2} \right) \int_{\ell_b}^x \frac{h_o^2 dx}{h^3(x)} \quad (7b)$$

$$s = \begin{cases} +1, & \text{for } x = [\ell_b, \ell_m] \\ -1, & \text{for } x = (\ell_m, \ell_t] \end{cases} \quad (7c)$$

$$s = \begin{cases} -1 & \text{assembly} \\ +1 & \text{disassembly} \end{cases} \text{ when } x = \ell_m$$

where $h(x)$ is defined in Eq. (1) and $H_x = h_x/h_o$. In Eq. (7), the sign s accounts for the direction of the induced moment, and at $x = \ell_m$, it takes the direction of the matching part defined in Fig. 1, positive for disassembly and negative for assembly.

2.2 Solution to Forward Model for Assembly. The normalized beam deflection $\Delta = \delta/h_o$ in Eq. (3) can be compactly written as

$$\Omega = \Delta/F_y = \Omega_+ + s(f_x/f_y)\Omega_- \quad (8)$$

In Eq. (8), Ω_+ and Ω_- are defined in Eqs. (5) and (7), respectively. The dimensionless mechanical impedances (Ω_{1+} , Ω_{2+} , Ω_{3+}) and (Ω_{1-} , Ω_{2-}) for the geometry in Fig. 2 are given in the Appendix. The inverse model, which determined F_y in Eq. (8) for a given deflection and force ratio f_x/f_y in Eq. (2b), can be solved in closed form

$$\text{Inverse model : } F_y = \frac{\Delta}{\Omega_+ + s(f_x/f_y)\Omega_-} \quad (9a)$$

The forward model which explicitly solves for the overall impedance ($\Omega = \Delta/F_y$) must account for the force ratio f_x/f_y (which depends on contact location and deflection and hook geometry) and is rewritten from Eq. (8) as

$$\text{Forward model : } \eta \left(\frac{F_y}{X} \right) \Omega^2 - \left[\left(\frac{F_y}{X} \right) (\eta \Omega_+ - s \Omega_-) + \sigma \right] \Omega + \sigma(\Omega_+ + s \eta \Omega_-) = 0 \quad (9b)$$

$$\text{where } \eta = \begin{cases} \tan(\gamma + \beta_c) & \text{Insertion and Dwelling} \\ \tan(\gamma - \beta_c) & \text{Retention} \end{cases} \quad (10a)$$

$$\sigma = \begin{cases} 1, & \text{Insertion and dwelling} \\ -1, & \text{Retention} \end{cases} \quad (10b)$$

$$s = \begin{cases} +1, & \text{for } x = [\ell_b, \ell_m] \\ -1, & \text{for } x = [\ell_m, \ell_t] \end{cases} \quad (10c)$$

In Eq. (10a),

$$\beta_c = \tan^{-1} \mu \quad (10d)$$

$$\gamma = \begin{cases} \alpha, & \text{for } x = [\ell_m, \ell_t] \\ \beta, & \text{for } x = [\ell_b, \ell_m] \end{cases} \quad (10e)$$

The closed-form solution to Eq. (9b) is given by Eq. (11) where Ω must be real ($4ac/b^2 \leq 1$)

$$\Omega = \frac{b}{2a} \left[1 \pm \sqrt{1 - ac(2/b)^2} \right] \quad (11)$$

$$\text{where } a = \eta F_y / X \quad (11a)$$

$$b = (\eta\Omega_+ - s\Omega_-)F_y/X + \sigma \quad (11b)$$

$$c = \sigma(\Omega_+ + s\eta\Omega_-) \quad (11c)$$

2.3 Effects of Simplified Models on Assembly Force Calculations. The overall deflection is contributed by component impedances ($\Omega_{1+}, \Omega_{2+}, \Omega_{3+}$) in Eqs. (5a)–(5c) due to the vertical force and (Ω_{1-}, Ω_{2-}) in Eqs. (7a) and (7b) due to horizontal induced moment, where $\Omega_{1\pm}$ and $\Omega_{2\pm}$ are computed on the uniform section and the hook shape of the cantilever beam, respectively, and Ω_{3+} accounts for the shear deformation. The magnitudes of these component impedances as a percentage of ($\Omega_+ + \Omega_-$) are compared in Fig. 2 where the hook dimensions are $\alpha = 45$ deg, $\beta = 90$ deg, and $H_b = 1$, and data were computed at $X = L_b + 0.5$ for insertion. The magnitudes of Ω_{1+} and Ω_{1-} , which, respectively, increases and decreases with L_b , are generally significantly higher than those of Ω_{2+} , Ω_{3+} , and Ω_{2-} . These straight-forward comparisons often lead designers to simplify analyses by neglecting the hook geometry or approximate it as an Euler–Bernoulli beam which assumes no shear deformation ($G \rightarrow \infty$), $K = 1$, and $\Omega_{3+} = 0$ in Eq. (5).

Two commonly used simplified models are discussed here.

1. A common design practice is to treat the cantilever hook as a uniform beam and neglect the bending moment M . The result is essentially the first term in Eq. (5a) with $L_b \rightarrow L_t$.

$$\text{Simplified model 1 (SM1)}: \quad \Omega = \Delta/F_y \approx (4KL_x^3) \quad (12)$$

The hook geometry [h_b, α, β] cannot be accounted for when Eq. (12) is used.

2. A second approximation accounts for the hook geometry but neglects the horizontally induced moment M .

$$\text{Simplified model 2 (SM2)}: \quad \Omega = \Delta/F_y \approx \Omega_+ = 4KL_b^3 + \Omega_{2+} + \Omega_{3+} \quad (13)$$

This is a special case of Eq. (9b) when $F_y/X \ll 1$ and $\eta \approx 0$. As in SM1, SM2 neglects the effects of friction and f_x .

Figure 3 illustrates the effect of model approximation on the deflecting force for assembling the snap-fit 1 with dimensions given in Table 1. Computed using SM1 and SM2 for “Insertion,” “Dwelling,” and “Retention,” the results are compared against the CM or Eq. (9a), which accounts for the hook geometry and bending moment with shear deformation. Two observations in Fig. 3 are discussed.

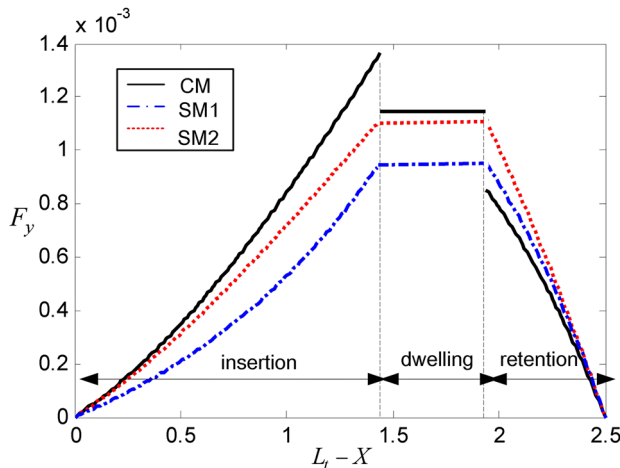


Fig. 3 Comparing SM1 and SM2 against CM

Table 1 Characteristic dimensions of snap-fit 1

α	β	L_t	L_b	H_b	L_m	μ
25 deg	50 deg	7	5	0.67	5.56	0.1

- The induced moment due to f_x is negative (or $s = -1$) when $x \in (\ell_m, \ell_t]$ during insertion and must be overcome when deflecting the beam. Both simplified models which neglect this effect grossly underestimate the deflecting force. On the other hand, the induced moment is positive (or $s = +1$) when $x \in [\ell_b, \ell_m)$, which tends to deflect the beam during the process of retention; as a result, both simplified models overestimate the deflecting force.
- At the instant when the process changes from insertion to dwelling, the force ratio f_x/f_y suddenly increases in value to μ . Similarly, the deflecting force drops when transitioning from dwelling to retention. Both these two discontinuities, insertion-to-dwelling and dwelling-to-retention, cannot be accounted for by either SM1 or SM2.

2.4 Design Analyses for Disassembly. Disassembly of snap-fits follows similar derivations for assembly except that the matching part moves from $(x, y) = (\ell_b, -h_b/2)$ in the $+x$ direction. For calculating the forward and inverse solutions in disassembly from Eqs. (11) and 9(a), Insertion, Dwelling, and Retention in Eqs. (2b) and (10a) are replaced with “Detachment,” “Dwelling,” and “Release” which occur in sections $x = [\ell_b, \ell_m), \ell_m, (\ell_m, \ell_t]$ with slope angles $\gamma = \beta, 0, \alpha$, respectively.

Figure 4 shows the normalized assembly force F_x involved in a typical cycle of assembly and disassembly of a snap-fit (dimensions given in Table 1). When $x \in (\ell_m, \ell_t]$, the frictional force opposes the motion of the matching part as it slides upward along the sloping surface of the deflected hook during assembly but acts in the opposite direction during disassembly. As derived in Eq. (2b), the force ratio f_x/f_y equals to $\tan(\gamma' + \tan^{-1} \mu)$ during assembly while it equals to $\tan(\gamma' - \tan^{-1} \mu)$ during disassembly. Thus, for the same slope (with angle $\gamma' = \alpha'$), the required insertion force during assembly is larger than that required for release as shown on the left half of Fig. 4. Similar arguments can be made on $x \in [\ell_b, \ell_m)$ with slope angle β , where the required detaching force is larger than retention force. Recall Eq. (7c) that $s = -1$ for assembly and $+1$ for disassembly during dwelling; $F_x = \mu F_y$ for assembly is slightly higher than that for disassembly as given in Eq. (8).

- (1) When $\beta < \beta_c (= \tan^{-1} \mu)$, the ratio (f_x/f_y) in Eq. (2b) is negative in retention. In practice, it implies that the

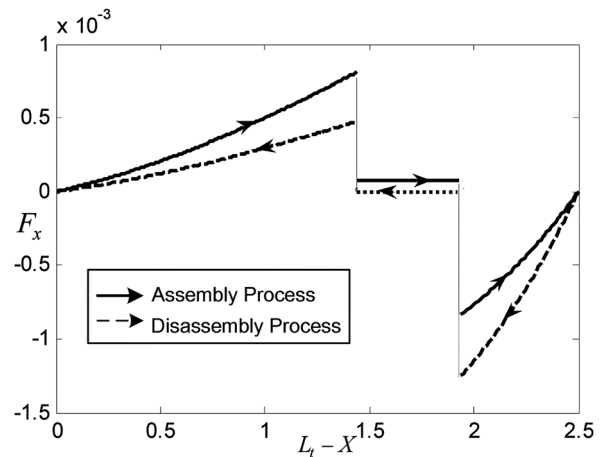


Fig. 4 Forces computed using CM for assembly and disassembly

cantilever hook will never rebound to the original nondeformed position; the cantilever hook cannot be disassembled. When $\mu > \cot \beta$ during insertion, the ratio (f_x/f_y) in Eq. (2b) is negative, which means cantilever hook is too steep to be disassembled.

- (2) When $\beta \rightarrow \pi/2$ (and $\mu \approx 0$) such that $\eta \rightarrow +\infty$ during detachment, Eq. (9b) becomes independent of η and reduces to

$$F_y = \Delta^2(\Delta\Omega_+ + X\Omega_-)^{-1} \quad (14)$$

Noting that $H_x = H_b$ at $X = L_m$, the required force to deflect the beam by $\Delta = H_b$ is thus given by

$$|F_y(X = L_m)| = \frac{H_b^2}{(4KH_b + 6H_b + 3)L_m^3}$$

The cantilever hook can only be unlocked with F_y . A common application is an automatic switch (such as a circuit breaker for mechanical equipment or power control), which is normally in contact and breaks open to cut off current automatically when short circuit occurs.

3 Results and Discussions

Three sets of results are discussed here. The first set numerically compares computed results against two different methods for verifying the model validation. The second set illustrates the use of the models for identifying the friction coefficient. The experimental results (obtained from three different design configurations (DCs) with surface materials) offer a means to validate the models. The third set demonstrates a unique application where the closed-form solutions are used for haptic rendering during design.

3.1 Model Verification. The accuracy of the model has been verified by comparing results against two different methods: a three-dimensional FEM implemented on ANSYS workbench [17] and an approximate solution in Ref. [9]. The values of geometrical and FEM parameters and material properties used in simulating the snap-fit 2 for these comparisons, which are exactly the same as in Ref. [9], are given in Table 2. The results are compared in Fig. 5, where we define the matching part displacement x' so that comparisons can be made on the same coordinate

$$x' = \ell_t - \left[\frac{\ell_b}{2} + \sqrt{\left(x - \frac{\ell_b}{2}\right)^2 + \delta^2} \right] \quad (15)$$

Equation (8) has been derived with the assumption that θ is small and that the length of $\ell_t - x'$ approximately composes of $\ell_b/2$ and the hypotenuse $\sqrt{(x - \ell_b/2)^2 + \delta^2}$. Unlike the JK approximation [9] which neglects the deflection due to the horizontal moment given in Eq. (6), the proposed method agrees well with the FEA as compared in Fig. 5.

Table 2 Geometrical parameters, material properties FEM of snap-fit 2

Geometry	Materials	Elements in ANSYS
α, β (deg)	45,90	E(MPa) 2400
ℓ_t (mm)	57.5	ν 0.45
ℓ_b (mm)	50	μ 0
ℓ_m (mm)	50	Beam: SOLID 186
h_o (mm)	2.5	Contact: CONTA174, TARGE170
h_b (mm)	7.5	Number of elements: 7086
w (mm)	5	Substeps number to 1s : 102
		Mapped meshing method

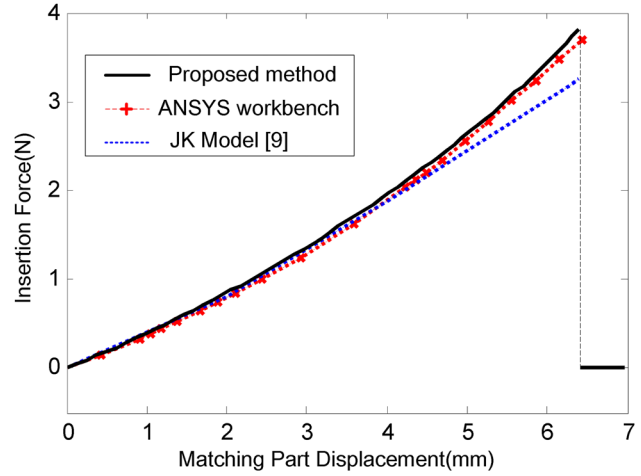


Fig. 5 Insertion force versus displacement

3.2 Estimation of Friction Coefficient Using an “Outlet.”

Figure 6(a) demonstrates the use of an outlet (commonly in household products) to determine the friction coefficient between two material surfaces of a snap-fit. As compared in Fig. 6(b), three different outlet design configurations (DCs) are illustrated here as a means of experimental validation, each of which consists of a cold-drawn brass plug ($E = 0.93$ GP and $\nu = 0.35$) and a fixed socket made of rolled phosphor bronze ($E = 1.13$ GP and $\nu = 0.41$). The extraction of the plug from the socket is essentially the dwelling process of a snap-fit, and thus follows Eq. (2b) or $f_x/f_y = \mu$ which can be used to determine the friction coefficient between the two different material (socket and plug) surfaces. Thus, from Eq. (8) with $s = +1$

$$\mu = \frac{\Omega_+}{\Delta/F_x - \Omega_-} \quad \text{where} \quad \frac{\Delta}{F_x} = Ew \frac{\delta_{\max}}{f_x} \quad (16)$$

In Eq. (16), the critical value of f_x can be determined experimentally by gradually increasing the weight (mg) until the plug slips off the socket as shown in Fig. 6(a); Ω_+ and Ω_- are given by Eqs. (5) and (7), respectively, and the maximum deflection δ_{\max} can be determined from the thickness of the plug. The experimentally determined critical f_x and the corresponding computed friction coefficient are given in Table 3.

Since the three different outlet designs are made of the same materials, they should theoretically have the same friction coefficient. The root-mean-square value of the three friction coefficients (0.123, 0.136, and 0.142) obtained experimentally from three different outlet designs is 0.134. The maximum difference is within 5% of the root-mean-square value.

3.3 Haptic Evaluation. It is desired that realistic force feedback can be felt virtually by designers when optimizing geometry. This can be achieved by means of a haptic device (PHANTOM [16]) incorporating the sense of touch and control into the computer as illustrated in Fig. 7.

3.3.1 Design Options. Performance of cantilever hook is determined by various parameters. For the detachable snap-fits, users prefer to assemble with “least effort” (or the minimum insertion force $|f_x|$) while allowing for ease of disassembly. This represents a design trade-off between the insertion and the retention angles for a specified hook length ($\ell_t - \ell_b$) and offset h_b . Thus, several combinations of different insertion and retention angles with the same maximum offset are considered here and presented in Table 4. As an illustration, the design objective here focuses to determine a preferred set of α and β .

Assembly feedback force is calibrated using a set of forces (5, 10, 15, and 20 N) to permit the designer to distinguish discrete

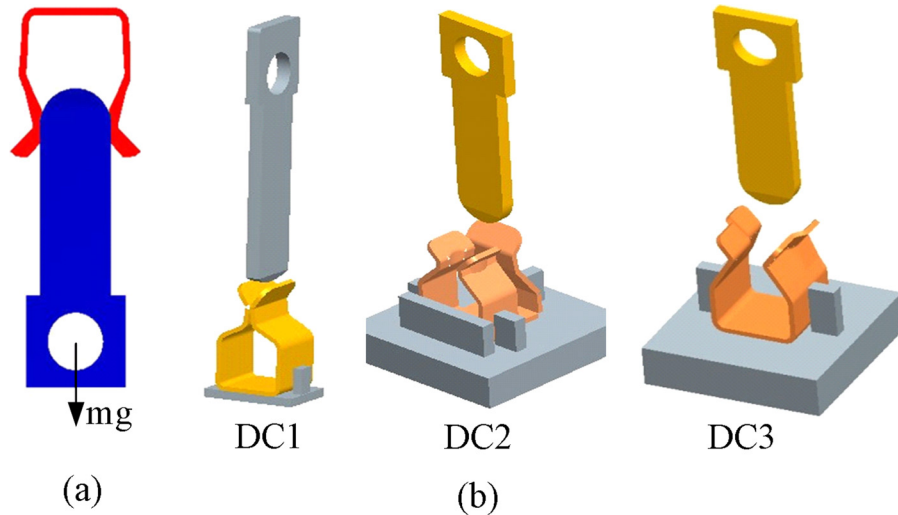


Fig. 6 Outlet design configurations and friction coefficient; (a) determining μ and (b) three different outlet design configurations

Table 3 Experimental data for calculating friction coefficient

Type	DC1	DC2	DC3
Socket (mm)	$\ell_b = 5, \ell_m = 6.9, \beta = 60 \text{ deg},$ $h_b = 3.2, h_o = 0.5, w = 7$	$\ell_b = 3.0, \ell_m = 7.1, \beta = 35.3 \text{ deg},$ $h_b = 2.5, h_o = 0.6, w = 6.8$ width = 6.3, thickness = 1.5	$\ell_b = 5.4, \ell_m = 9.6, \beta = 58.8 \text{ deg},$ $h_b = 1.8, h_o = 0.6, w = 8$
Plug (mm)			
Deflection (mm)	$\delta_{\max} = 0.75$	$\delta_{\max} = 1.2$	$\delta_{\max} = 0.75$
Critical f_x (N)	160 g	1070 g	260 g
μ	0.136	0.123	0.142

steps of forces for a specified set of design values (including material and geometry parameters). For the detachable snap-fit, the assembly force $f_a < 10 \text{ N}$ and disassembly force $f_d > 10 \text{ N}$. With these constraints, nine design options listed in the first four columns in Table 4 are chosen as inputs to the haptic algorithm.

3.3.2 *Inverse Model for Haptic Rendering.* For real-time applications, rapid haptic feedback is achieved using embedded algebraic solutions given in Sec. II. The solutions to the forward model (9b), however, compute the mechanical impedances for

snap-fit design (geometry and material) for a given contact point and force. Haptic rendering, which can enhance the snap-fit design for assembly, requires the feedback of virtual forces in real time and thus the solutions to the inverse model which computes the force from the deflection and contact position. Once the location X (and hence the deflection Δ) of the matching part is given, the deflecting force f_y can be computed from Eq. (8), and the corresponding assembly/disassembly force f_x can be obtained from Eq. (2b).

3.3.3 *Haptic Interface and Human Force.* The Haptic Device API [16] is employed here to enable the designer to obtain feedback force information in real time directly with the assistance of SENSABLE OPENHAPTICS. In Fig. 7, the position of PHANTOM stylus as carrier for moving object is detected in high frequency (1 kHz). Users evaluate the reaction force in virtual environment. The feedback forces for the nine different cantilever design options have been recorded (Fig. 8) while experienced by users with the assistance of haptic device. In Fig. 8, the horizontal and vertical axes represent the displacement of the matching part and the feedback force, respectively.

Nine individuals participated as design evaluators with the aid of the haptic device. Each evaluator experienced a “haptic” feeling of the insertion force, retention force, and the abrupt change while the insertion angle was stepped up from 18.5 until 45. The nine different labeled design options (Table 4) were randomized before each blindfolded evaluator conducted the sequential evaluation of the nine design configurations to determine the preferred option; only one trail was allowed for each evaluator. Note that beta is dependent on alpha for a specified $l_b, h_b,$ and l . When beta equals to 90 deg, 76.6 deg, 69.2 deg, 63 deg, 57.8 deg, and 53.5 deg, the corresponding alpha values are 18.5 deg, 20 deg, 21 deg, 22 deg, 23 deg, and 24 deg. As shown in Fig. 8, there are significant differences in insertion and detaching forces among some

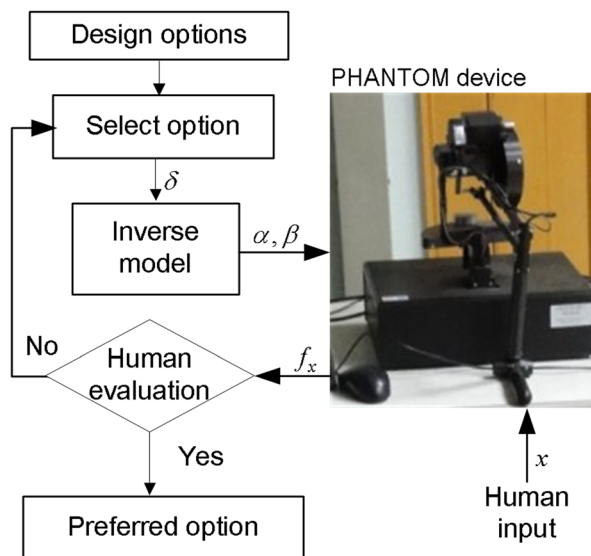


Fig. 7 Haptic evaluation procedure

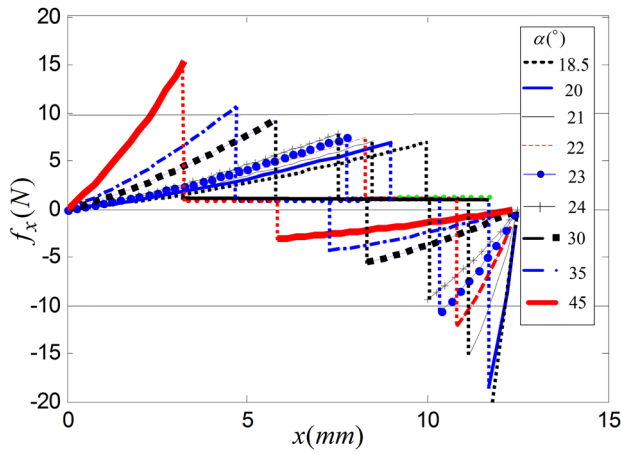


Fig. 8 Haptic feedback curve

(α , β) combinations. Although there appears little differences among the insertion forces for the designs with insertion angles of 18.5 deg, 20 deg, 21 deg, 22 deg, 23 deg, and 24 deg, the detaching forces differ significantly (as shown in Fig. 8) from each other.

The results are given in the last two columns in Table 4, which aim at satisfying two constraints: $f_a < 10$ N and $f_d > 10$ N. As seen in Fig. 8, options I–VII satisfy constraint $f_a < 10$ N, while options I–V satisfy constraint $f_d > 10$ N. In other words, only options I–V satisfy both these constraints, and based on the rule of least effort, option V is chosen as the optimal design. Two of the users chose option IV; it is worth noting that the felt force difference between option IV and option V is less than 5 N.

4 Conclusions

An analytical model for design cantilever hook has been presented, which has potential for applications where real-time haptic evaluation through feedback force of a human–computer interfacing mechanism is essential or represents an advantage. This relatively complete model, which takes into account the hook-shape geometry and the effect of shear deformation which cannot be neglected for thick elements, provides a basis for justifying assumptions made to neglect certain factors in applications where

Table 4 Design options and users' selection

$E = 0.24GPa$, $h_b = 3.35$, $\mu = 0.1$

	Design options		Geometry (mm)	User choice	Evaluation conclusion
	α	β			
I	18.5	90		V	
II	20	76.6	$l_t = 35$	V	78% users
III	21	69.2	$l_b = 25$	V	select option V
IV	22	63.0		VI	as preferred
V	23	57.8		V	option, while
VI	24	53.5	$w = 10$	V	the remainder
VII	30	38.6	$h_o = 5$	VI	selects
VIII	35	32.7		V	option VI.
IX	45	26.7		V	

simplified models may be desired to facilitate design optimization and real-time control. The relation between feedback force and deflection has been deduced illustrating a complete cycle of snap-fit assembly and disassembly; the results offer some insightful findings by comparing several commonly used simplified models.

The model presented has been verified by comparing against results obtained by ANSYS FEA workbench and published approximations and applied to two applications. The first illustrates its use to determine the friction coefficient between two contact surfaces. For this, the friction coefficient involved in three different designs (with same materials) was compared which closely agree within 5% of their root-mean-square value. The second demonstrates the effectiveness of the inverse model (as embedded algebraic solutions) for use in haptic rendering in design processes, where real-time virtual force feedback is essential. Implemented through a commercial PHANTOM haptic device, nine individuals participated in evaluating nine design options with different parameters settings. The experiment showed that 78% of them chose the optimal theoretical solution by feeling the feedback force. Through a relatively accurate virtual force feedback, it is expected that the confidence of assembly robustness can be enhanced in industrial settings.

Acknowledgment

The paper was supported by Major State Basic Research Development Program of China (No.2011CB706506) and the National Natural Science Foundation of China (No.50775201).

Nomenclature

Symbols

- A = beam cross-sectional area
- E = Young's modulus
- f = force
- F = normalized f
- G = shear modulus
- $h(x)$ = cantilever hook thickness along x
- h_b = height of the wedge-shaped hook
- H_b = normalized h_b
- h_o = base thickness of the cantilever hook
- I = moment of inertia
- k = dimensionless section shape coefficient
- l_b = beam length
- L_b = normalized l_b
- l_m = distance between hook tip and beam root
- L_m = normalized l_m
- l_t = cantilever hook length
- L_t = normalized l_t
- M = moment
- s = direction of the induced moment
- V = strain energy
- w = cantilever hook width
- x, y = contact point coordinates defined at beam root
- X, Y = normalized x and y

Greek Symbols

- α, β = initial wedge-shaped hook angles
- α', β' = deflected wedge-shaped hook angles
- β_c = friction angle
- δ = beam deflection
- Δ = normalized δ
- γ, γ' = initial and deflected angle defined in Eq. (2a)
- η = global equivalent friction coefficient
- μ = local friction coefficient
- θ = beam neutral axis deflection angle
- σ = the direction of the matching part moving
- v = passion ratio
- Ω = mechanical impedance

Subscripts

- x, y = along x or y direction
 n = normal to the slope surface
 s = parallel along the slope surface
 $+$ = positive y direction under deflection
 $-$ = negative y direction under deflection
 a = assembly
 d = disassembly
 ε = strain
max = maximum value

Appendix

The integrals in Eqs. (5b), (5c), and (7b) can be analytically solved by noting that

$$\int_{x_1}^{x_2} \frac{x^2 dx}{(a+bx)^3} = \frac{1}{b^3} \left[\ln|a+bx| + \frac{2a}{a+bx} - \frac{a^2}{2(a+bx)^2} \right] \Bigg|_{x_1}^{x_2}$$

$$\Omega_{2+} = \left\{ \begin{array}{l} \frac{6}{\tan^3 \beta} \left\{ -2 \ln \rho(h_o) - 4H_b \rho(h_o)(1 - L_b \tan \beta) + \right. \\ \left. H_b(2 + H_b)(1 - L_b \tan \beta)^2 \rho^2(h_o) \right\} - \frac{6}{\tan^3 \alpha} \left\{ 2 \ln \rho(r) + 4(1 + L_t \tan \alpha)(\rho(x) - \rho(h_o)) - \right. \\ \left. (1 + L_t \tan \alpha)^2 (\rho^2(x) - \rho^2(h_o)) \right\} \end{array} \right\} \begin{array}{l} \text{Insertion and} \\ \text{dwelling} \\ \\ \text{Retention} \end{array} \quad (\text{A2})$$

$$\Omega_{3+} = \left\{ \begin{array}{l} -\frac{kE}{G} \left[\frac{\ln \rho(r)}{\tan \alpha} + \frac{\ln \rho(h_o)}{\tan \beta} \right] \\ -\frac{kE}{G} \frac{\ln \rho(x)}{\tan \beta} \end{array} \right\} \begin{array}{l} \text{Insertion and dwelling} \\ \\ \text{Retention} \end{array} \quad (\text{A3})$$

$$\Omega_{2-} = \left\{ \begin{array}{l} \frac{3X}{2} (2H_x + 1) \left\{ \frac{\rho^2(x) - \rho^2(h_o)}{\tan \alpha} - \frac{\rho^2(h_o) - 1}{\tan \beta} \right\} \\ \frac{3X}{2 \tan \beta} (2H_x + 1) (1 - \rho^2(x)), \end{array} \right\} \begin{array}{l} \text{Insertion and dwelling} \\ \\ \text{Retention} \end{array} \quad (\text{A5})$$

References

- [1] Bonenberger, P. R., 2000, *The First Snap-Fit Handbook: Creating Attachments for Plastics Parts*, Hanser Gardner Publications, Cincinnati, OH.
- [2] AlliedSignal Corporation, 1997, *Modulus Snap-Fit Design Manual*, Allied-Signal Plastics, Morristown, NJ.
- [3] Bayer Corporation, 1996, *Snap-Fit Joints for Plastics, A Design Guide*, Polymer Division, Pittsburgh, PA.
- [4] Luscher, A. F., 1996, "Part Nesting as a Plastic Snapfit Attachment Strategy," *Proceedings of the 1996 54th Annual Technical Conference Part 1 (of 3)*, Indianapolis, IN, pp. 1302–1306.
- [5] Genc, S., Messler, R. W., and Gabriele, G. A., 2000, "A Method for Attachment Design Concept Development in Integral Snap-Fit Assemblies," *ASME J. Mech. Des.*, **122**(3), pp. 257–264.
- [6] Suri, G., and Luscher, A. F., 2000, "Structural Abstraction in Snap-Fit Analysis," *ASME J. Mech. Des.*, **122**(4), pp. 395–402.
- [7] Suri, G., and Luscher, A. F., 2006, "Development of Analytical Model of Cantilever Hook Performance," *ASME J. Mech. Des.*, **128**(2), pp. 479–493.
- [8] Lan, C., and Lee, K. M., 2008, "An Analytical Contact Model for Design of Compliant Fingers," *ASME J. Mech. Des.*, **130**(1), 011008.
- [9] Jorabchi, K., and Suresh, K., 2009, "Nonlinear Algebraic Reduction for Snap-Fit Simulation," *ASME J. Mech. Des.*, **131**(1), 061004.
- [10] Rusli, L., Luscher, A., and Sommerich, C., 2010, "Force and Tactile Feedback in Preloaded Cantilever Snap-Fits Under Manual Assembly," *Int. J. Ind. Ergon.*, **40**(6), pp. 618–628.
- [11] Rose, D., Bidmon, K., and Ertl, T., 2004, "Intuitive and Interactive Modification of Large Finite Element Models," *IEEE Visualization 2004 Conference*, Austin, TX, pp. 361–368.
- [12] Yang, Z. Y., Lian, L. L., and Chen, Y. H., 2005, "Haptic Function Evaluation of Multi-Material Part Design," *Comput.-Aided Des.*, **37**, pp. 727–736.
- [13] Feng, H., 2007, "Robot-Assisted Suspension Laryngoscopy Virtual Simulation System," Ph.D. thesis, Tianjin University, Tianjin, China.
- [14] Gao, Z., and Lecuyer, A., 2009, "Path-Planning and Manipulation of Nanotubes Using Visual and Haptic Guidance," *IEEE International Conference on Virtual Environments, Human-Computer Interfaces and Measurements Systems*, Hong Kong, China.
- [15] Wang, L., Wang, H. G., and Pen, Q. S., 2009, "Calculation and Tactile Perception for Molecular Force Field With CHARMM-Based Field," *J. Comput. Appl.*, **21**(7), pp. 886–893.
- [16] OPENHAPTICS® Toolkit version 3.0 Programmer's Guide.
- [17] ANSYS, Inc., www.ansys.com.